The many faces of blazar emission in the context of hadronic models

Maria Petropoulou[1], Stavros Dimitrakoudis[2], Paolo Padovani[3], Elisa Resconi[4], Paolo Giommi[5] and Apostolos Mastichiadis[6]

[1] *Department of Physics and Astronomy, Purdue University, West Lafayette, IN 47907, USA*
[2] *Department of Physics, University of Alberta, Edmonton, Alberta, Canada*
[3] *European Southern Observatory, D-85748 Garching bei München, Germany*
[4] *Technische Universität München, D-85748 Garching bei München, Germany*
[5] *ASI Science Data Center, via del Politecnico s.n.c., I-00133 Roma Italy*
[6] *Department of Physics, University of Athens, 15783 Zografos, Greece*

arXiv:1601.06010v1 [astro-ph.HE] 22 Jan 2016

We present two ways of modeling the spectral energy distribution of blazars in the hadronic context and discuss the predictions of each "hadronic variant" on the spectral shape, the multi-wavelength variability, the cosmic-ray flux, and the high-energy neutrino emission. Focusing on the latter, we then present an application of the hadronic model to individual BL Lacs that were recently suggested to be the counterparts of some of the IceCube neutrinos, and conclude by discussing the contribution of the whole BL Lac class to the observed neutrino background.

Keywords: astroparticle physics, neutrinos, radiation mechanisms: non-thermal, galaxies: BL Lacertae objects: general

1. Introduction

Blazar jets have long been considered as candidate sites of cosmic-ray acceleration to the highest energies observed ($\sim 5 \times 10^{20}$ eV). In the light of the recent IceCube neutrino detections, the hadronic model for blazar emission becomes more relevant than ever before. We compare the predictions of two variants of hadronic models for the the blazar spectral energy distribution (SED) by using the nearby BL Lac Mrk 421 as our testbed.

2. The Model

We adopt a one-zone leptohadronic model for the blazar emission, where the low-energy emission of the blazar SED is attributed to synchrotron radiation of relativistic electrons and the observed high-energy (GeV-TeV) emission is assumed to have a photohadronic origin.

We assume that the region responsible for the blazar emission can be described as a spherical blob of radius R, containing a tangled magnetic field of strength B and moving towards us with a Doppler factor δ. Protons and (primary) electrons are assumed to be accelerated into power-law energy distributions and to be subsequently injected isotropically in the volume of the blob with a constant rate. All particles are assumed to escape from the emitting region in a characteristic timescale, which is set equal to the photon crossing time of the source, i.e. $t_{\rm p,esc} = t_{\rm e,esc} = R/c$.

Photons, neutrons and neutrinos (ν_μ, ν_e) complete the set of the five stable populations, that are at work in the blazar emitting region. Pions ($\pi^\pm, \pi^0$), muons ($\mu^\pm$) and kaons ($K^\pm, K^0$) constitute the unstable particle populations, since they

decay into lighter particles. The production of pions is a natural outcome of photohadronic interactions between the relativistic protons and the internal photons; the latter are predominantly synchrotron photons emitted by the primary electrons. The decay of $\pi^{\pm}$ results in the injection of secondary relativistic electron-positron pairs ($\pi^+ \rightarrow \mu^+ + \nu_\mu$, $\mu^+ \rightarrow e^+ + \bar{\nu}_\mu + \nu_e$), whose synchrotron emission emerges in the GeV-TeV regime, for a certain range of parameter values. π^0 decay into very high energy (VHE) γ-rays (e.g. $E_\gamma \sim 10$ PeV, for a parent proton with energy $E_p = 100$ PeV), and those are, in turn, susceptible to photon-photon ($\gamma\gamma$) absorption and can initiate an electromagnetic cascade[1]. As the synchrotron self-Compton emission from primary electrons may also emerge in the GeV-TeV energy band, the observed γ-ray emission can be totally or partially explained by photohadronic processes, depending on the specifics of individual sources[2].

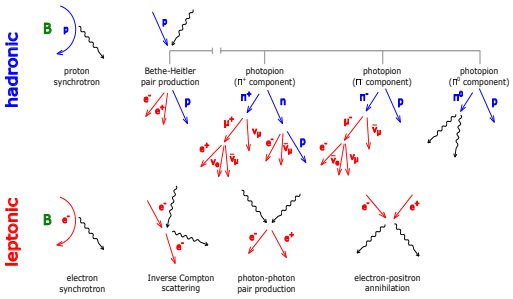

Fig. 1. Schematic illustration of the main hadronic and leptonic processes that are included in our numerical treatment.

The interplay of the processes (see Fig. 1) governing the evolution of the energy distributions of the five stable particle populations is formulated with a set of five time-dependent, energy-conserving kinetic equations. To simultaneously solve the coupled kinetic equations for all particle types we use the time-dependent code described in Ref. 3.

3. Hadronic Modeling Of The BL Lac Mrk 421

Mrk 421 is one of the nearest ($z = 0.031$) and brightest BL Lac sources in the VHE ($E_\gamma > 200$ GeV) sky and extragalactic X-ray sky, which makes it an ideal target of multi-wavelength observing campaigns. Using Mrk 421 as our testbed, we present two ways of modeling the blazar SED in the hadronic context, namely the LHπ and LHs models. Table 1 summarizes the main features of those models, while details about the spectral shape and variability, the neutrino and cosmic-ray emission are presented in the following paragraphs.

3.1. *Photon, neutrino and cosmic-ray spectra*

In the LHπ model (Fig. 2, left panel) the proton synchrotron emission is suppressed, whereas the photopair and photopion components are prominent. This is the result of a low magnetic field in combination with a high proton luminosity. The SED does not have the usual double-humped appearance as synchrotron photons from the photopair secondaries produce a broad hump at MeV energies (see also Ref. 4).

Table 1. Comparison of the hadronic model variants LHπ and LHs.

	LHπ model	LHs model
UV-to-X-rays	primary e^- synchrotron	primary e^- synchrotron
GeV-to-TeV γ-rays	secondary e^- synchrotron	p synchrotron
Dominant energy density	proton	magnetic
Jet power (erg/s)	$\sim 10^{48}$	$\sim 10^{46}$
Maximum proton energy	~ 20 PeV	~ 20 EeV
Maximum neutrino energy	~ 1 PeV	~ 1 EeV
X-ray flux vs. TeV flux	quadratic	linear

The energetic requirements of this model are high (see Table 1), while most of the energy is carried by the highest energy particles. Although the radiative efficiency of the model is low ($\sim 10^{-5}$), the high proton luminosity leads to a substantial neutrino flux that is of the same order as the TeV rays. Interestingly, the expected $\nu_\mu + \bar{\nu}_\mu$ flux, which peaks at ~ 3.3 PeV, is just under the sensitivity of the IC-40 detector (orange line). The cosmic-ray proton spectrum resulting from neutron decay peaks at 70 PeV (Fig. 2, right panel). This is just an upper limit of what it would appear at Earth since we have not taken into account CR diffusion, which is important for energies $< 10^{17}$ eV. At any rate, our values, even as an upper limit, are well below the observed CR flux at such energies. In the LHs model,

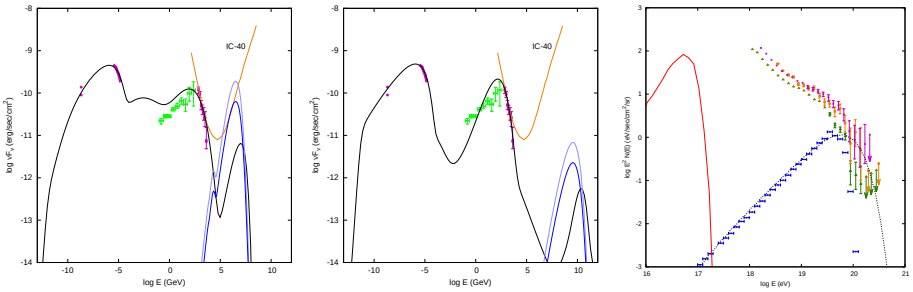

Fig. 2. *Left and middle panels*: spectra of photons (black line) fitting the March 22nd/23rd 2001 observation of Mrk 421 (purple points), neutrinos of all flavors (grey line) and $\nu_\mu + \bar{\nu}_\mu$ flux (thick blue line) according to the LHπ and the LHs models respectively. Fermi observations (green points) are not simultaneous with the rest of the data and thus not included in the fit. The 40-String IceCube limit[5] for ν_μ is plotted with an orange line. *Right panel*: cosmic-ray (proton) spectra resulting from neutron decay and obtained within the LHπ (red line) and LHs (blue dashed line) models. For the latter, the cosmic-ray spectra obtained after taking into account propagation effects using the numerical code CRPropa 2.0[6] are also shown (blue crosses). Different symbols are used for the cosmic-ray energy flux measurements by Auger, HiRes-I, and Telescope Array.

the high magnetic field coupled with a low proton injection luminosity leads to a suppressed photohadronic component. The SED has two well-defined peaks, both from synchrotron radiation of electrons and protons at UV/X-rays and GeV/TeV γ-ray energies, respectively. This also results in a low neutrino flux (a factor of 10

less than the TeV γ-ray flux). The peak of the neutrino flux emerges at energies of ~ 0.1 EeV due to the high values of the magnetic field and of the maximum proton energy (see Table 1). The higher value of the maximum proton Lorentz factor used in the SED fitting makes the discussion about ultra-high energy cosmic-ray (UHECR) emission more relevant. The propagation of UHE protons in a uniform intergalactic 1pG magnetic field and their energy losses from interactions with the cosmic microwave and infraredoptical backgrounds were modeled using CRPropa 2.0. The resulting spectra (blue crosses in right panel of Fig. 2) peak at ~ 60 EeV and they are just below the present UHECR flux limits in the energy range $30 - 60$ EeV.

3.2. *Variability*

Recently, the variability signatures expected in the framework of hadronic models have been studied in Ref. 7 by introducing small-amplitude variations to one (or more) model parameters around their time-averaged values. In particular, the temporal variations in the fitting parameter y were modeled as random-walk changes of the form $y_i \equiv y(t_i) = y_0\,(1 + 0.05\alpha_i)$, where $\alpha_{i+1} = \alpha_i + (-1)^{\kappa}$; here, κ is a uniformly distributed random integer number in the range (0,10). An indicative example is presented in Fig. 3, where the varying model parameters are the proton and primary electron injection luminosities. A strong correlation between the X-ray and TeV γ-ray fluxes is found in the LHπ model. Moreover, a quadratic relation between the TeV and X-rays fluxes is found, similarly to the leptonic SSC model. In the LHs model, the correlation is present but not as strong as in the LHπ model, while the TeV γ-rays vary linearly with respect to X-rays.

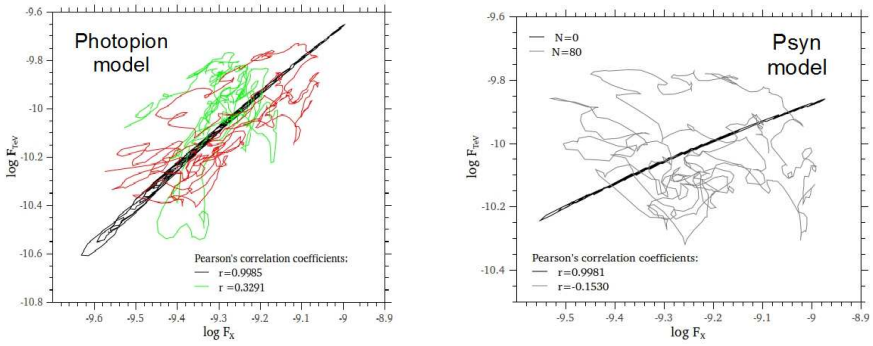

Fig. 3. TeV γ-ray flux vs. X-ray flux as obtained in the LHπ (left panel) and LHs (right panel) models by varying the injection luminosity of primary electrons and protons. We considered the cases of uncorrelated variations (green line) as well as of correlated variations with no time-lag (black lines) and a positive time-lag of $80t_{\rm cr}$ (red and grey lines in the left and right panels, respectively).

4. Neutrino emission from individual BL Lacs

In Ref. 8 the authors have recently searched for plausible astrophysical counterparts within the median error circles of IceCube neutrinos using a model-independent method and derived the most probable counterparts for 9 out of the 18 neutrino events of their sample. Interestingly, these include 8 BL Lac objects (6 with measured redshifts), amongst which the nearest blazar, Mrk 421, and two pulsar wind nebulae. The (quasi)-simultaneous SEDs of those 6 BL Lacs, namely Mrk 421, 1ES 1011+496, PG 1553+113, H 2356−309, 1H 1914−194, and 1RXS J054357.3−553206, were fitted[2] with the leptohadronic model described in Section 2. The all-flavor neutrino fluxes derived by the model are presented in Fig. 4(a). According to the model-independent analysis of Ref. 8, neutrino

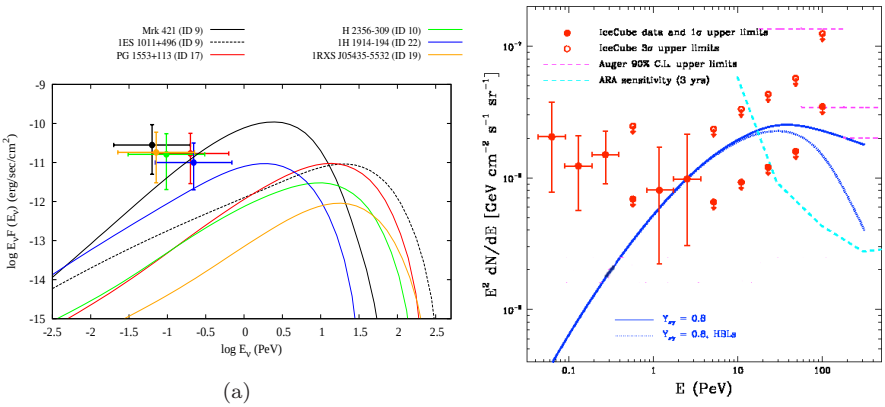
Mrk 421 (ID 9)
1ES 1011+496 (ID 9)
PG 1553+113 (ID 17)
H 2356-309 (ID 10)
1H 1914-194 (ID 22)
1RXS J05435-5532 (ID 19)
log E_ν F (E_ν) (erg/sec/cm^2)
log E_ν (PeV)
IceCube data and 1σ upper limits
IceCube 3σ upper limits
Auger 90% C.L. upper limits
ARA sensitivity (3 yrs)
E^2 dN/dE [GeV cm^-2 s^-1 sr^-1]
E (PeV)
Y_pγ = 0.8
Y_pγ = 0.8, HBLs

(a) (b)

Fig. 4. (a) Comparison of the model (lines) and the observed (circles) neutrino fluxes as defined in Ref. 7 for the six BL Lacs of the sample. The Poissonian 1σ error bars for each event are also shown. (b) The predicted neutrino background (per neutrino flavor) from all BL Lacs (blue solid line) and from high-frequency peaked BL Lacs (HBL) only (blue dotted line) for $Y_{p\gamma} = 0.8$ and $E_{\rm break} = 200$ GeV, $\Delta\Gamma = 0.5$. The curves correspond to the mean value of ten different simulations. The (red) filled points are the data points from Ref.[9], while the open points are the 3σ upper limits. The upper (magenta) short dashed line represents the 90% C.L. upper limits from Auger[10] while the lower (cyan) short dashed line is the expected three year sensitivity curve for the Askaryan Radio Array[11].

event 9 has two plausible astrophysical counterparts: the BL Lacs Mrk 421 and 1ES 1011+496. The differences between the neutrino fluxes originate from the differences in their SEDs. In this regard, the case of neutrino event 9 reveals in the best way how detailed information from the photon emission may be used to lift possible degeneracies between multiple astrophysical counterparts. As the neutrino spectrum for 1ES 1011+496 (dashed line in Fig. 4(a)) is an upper limit, our results strongly favor Mrk 421 against 1ES 1011+496.

In all cases, the model-derived neutrino flux at the energy bin of the detected

neutrino is below the 1σ error bars, but still within the 3σ error bars. Although the association of these sources cannot be, strictly speaking, excluded at the present time, blazars Mrk 421 and 1H 1914-194 are the two most interesting cases, because their association with the respective IceCube events can be either verified or disputed in the near future. Figure 4(a) demonstrates that the model-derived neutrino spectra from blazars with different properties are similar in shape. We may thus model the observed differential neutrino plus anti-neutrino ($\nu + \bar{\nu}$) flux of all flavors ($F_\nu(\epsilon_\nu)$) as $F_\nu(\epsilon_\nu) = F_0 \epsilon_\nu^\beta \exp\left(-\frac{\epsilon_\nu}{E_0}\right)$, where $\langle\beta\rangle \sim 0.34$ and E_0 is in good approximation equal to the peak energy of the neutrino spectrum, namely $\epsilon_{\nu,p}(\delta, z, \nu_{\rm s}) \simeq 17.5\,{\rm PeV}(1+z)^{-2}\,(\delta/10)^2\,\left(10^{16}{\rm Hz}/\nu_{\rm s}\right)$. In the above, δ is the Doppler factor, z is the source redshift and $\nu_{\rm s}$ is the *observed* synchrotron peak frequency. The luminosity from the photopion component is directly connected to that of $\sim 2 - 20$ PeV neutrinos. Thus, our approach allows us to associate the observed blazar γ-ray flux with the expected all-flavor neutrino flux as $F_{\nu,{\rm tot}} = Y_{\nu\gamma} F_\gamma\,(> E_\gamma)$, where $E_\gamma = 10$ GeV and $Y_{\nu\gamma}$ is a factor that includes all the details about the efficiency of photopion interactions; for example, $Y_{\nu\gamma} \ll 1$ implies an SSC origin for the blazar γ-ray emission. The normalization F_0 can be then inferred from the above.

5. The neutrino background from BL Lacs

The calculation of the neutrino background (NBG) from *all* BL Lacs requires detailed knowledge of the blazar population in terms of $\nu_{\rm s}$, δ, γ-ray fluxes and redshift. All these parameters, and many more, are available in the Monte Carlo simulations presented in a series of papers by Giommi & Padovani (e.g. Refs. 12, 13). We note that the blazar SEDs in the simulations are extrapolated to the VHE band by using the simulated *Fermi* fluxes and spectral indices and assuming a break at $E = E_{\rm break}$ and a steepening of the photon spectrum by $\Delta\Gamma$ (for details, see Ref. 13).

We assign to each blazar in the simulation a neutrino spectrum. Since E_0 is fully determined for a given set of $\delta, z, \nu_{\rm s}$ and β covers a narrow range, we are left only with $Y_{\nu\gamma}$ as a possible "tunable" parameter. Then, we compute the total NBG as $\int_{F_{\rm min}}^{F_{\rm max}} F\,(dN/dF)dF$ where dN/dF is the differential number counts and $F_{\rm min}, F_{\rm max}$ are the fluxes over which these extend. To obtain the NBG per neutrino flavor we divide our results by three. Finally, we perform ten simulations and calculate their average in order to smooth out the "noise" inherent to the Monte Carlo simulations.

The predicted NBG from BL Lacs is presented in Fig. 4(b) for $Y_{\nu\gamma} = 0.8$, $E_{\rm break} = 200$ GeV, and $\Delta\Gamma = 0.5$. We find that BL Lacs as a class (blue solid line) can easily explain the whole NBG at $E_\nu \gtrsim 0.5$ PeV, while they do not contribute much ($\sim 10\%$) at lower energies. At $E_\nu \lesssim 30$ PeV most of the contribution to the NBG comes from high-frequency peaked BL Lacs (HBL) (blue dotted line). Although HBL represent a small fraction ($\sim 5\%$) of the BL Lac population, they dominate the neutrino output up to ≈ 30 PeV due to their relatively high γ-ray, and therefore neutrino, fluxes and powers. According to preliminary calculations our results up to $\sim 1 - 2$ PeV are not sensitive on whether $Y_{\nu\gamma}$ is constant or

dependent on the blazar γ-ray luminosity. However, assuming an anti-correlation between $Y_{\nu\gamma}$ and $L_\gamma(>10\text{GeV})$, we find that the predicted NBG at $E_\nu \gtrsim 5$ PeV is in tension with the 3σ IceCube upper limits and the 90% C.L. upper limits from Ref. 10. Thus, this hypothesis is ruled out.

The model prediction on the detectability of 2 PeV$< \epsilon_\nu < 10$ PeV neutrinos for the NBG shown in Fig. 4(b) is $N_\nu \sim 4.6$ without taking into account the Glashow resonance (and $N_\nu \sim 7$, otherwise). This calculation is based on the effective areas from Ref. 14. Since the model NBG peaks at $\epsilon_\nu > 10$ PeV, we expect 2-3 additional events up to $\sim$ 100 PeV after making an educated guess on the effective areas above 10 PeV. Given that the 3σ upper limit for 0 events is 6.6[15], the prediction of $N_\nu \sim 6.6 - 7.6$ is close to being inconsistent with the IceCube non-detections. However, $Y_{\nu\gamma} = 0.8$ is likely an upper limit. This was derived, in fact, from a small sample of BL Lacs, which may represent the tip of the iceberg in terms of neutrino emission, as they were selected as the most probable candidates[8]. For example, if $Y_{\nu\gamma} = 0.3$ then we expect $N_\nu \approx 3$ (4) for $2 < \epsilon_\nu < 100$ PeV, which is well within the 2σ limit for 0 events.

Acknowledgments

M.P. acknowledges support for this work by NASA through Einstein Postdoctoral Fellowship grant number PF3 140113 awarded by the Chandra X-ray Center, which is operated by the Smithsonian Astrophysical Observatory for NASA under contract NAS8-03060. E.R. is supported by a Heisenberg Professorship of the Deutsche Forschungsgemeinschaft (DFG RE 2262/4-1).

References

1. K. Mannheim, P. L. Biermann and W. M. Kruells, *A&A* **251**, 723 (1991).
2. M. Petropoulou, S. Dimitrakoudis, P. Padovani, A. Mastichiadis and E. Resconi, *MNRAS* **448**, 2412 (2015).
3. S. Dimitrakoudis, A. Mastichiadis, R. J. Protheroe and A. Reimer, *A&A* **546**, A120 (2012).
4. M. Petropoulou and A. Mastichiadis, *MNRAS* **447**, 36 (2015).
5. C. Tchernin, J. A. Aguilar, A. Neronov and T. Montaruli, *A&A* **555**, A70 (2013).
6. K. H. Kampert et al., *APh* **42**, 41 (2013).
7. A. Mastichiadis, M. Petropoulou and S. Dimitrakoudis, *MNRAS* **434**, 2684 (2013).
8. P. Padovani and E. Resconi, *MNRAS* **443**, 474 (2014).
9. M. G.Aartsen et al., *Phys.Rev.Lett.* **113**, 10 (2014).
10. The Pierre Auger Collaboration, `arXiv:astro-ph.HE/1307.5059`, 2013
11. The ARA Collaboration, *APh* **35**, 457 (2012).
12. P. Giommi et al., *MNRAS* **420** 2899 (2012).
13. P. Padovani and P. Giommi, *MNRAS* **446**, L41 (2015).
14. M. G. Aartsen et al. *Phys.Rev.D* **88**, 11 (2013).
15. N. Gehrels, *ApJ* **303**, 336 (1986).